Malaysian Journal of Analytical Sciences (MJAS)
Published by Malaysian Analytical Sciences Society

SYNTHESIS OF HYBRID CARBON QUANTUM DOTS FROM *Tamarindus indica* AND *Mangifera indica* LEAVES FOR THE DETECTION OF MERCURY (Hg^{2+}) ION IN PURIFIED WATER AND SIMULATED SEAWATER

(Sintesis Titik Kuantum Karbon Hibrid dari Daun *Tamarindus indica* dan *Mangifera indica* bagi Pengesanan Ion Merkuri (Hg^{2+}) dalam Sampel Air Tulen dan Simulasi Air Laut)

Rejie C. Magnaye*, Riszel B. De Castro, Kenneth B. Gomez, Rex Gregor M. Laylo, Aljon Joseph G. Maderazo

Chemical and Food Engineering Department
College of Engineering, Architecture and Fine Arts
Batangas State University,
Golden Country Homes Subdivision, Alangilan, Batangas City, Philippines

**Corresponding author: rejie.magnaye@g.batstate-u.edu.ph*

Received: 16 July 2021; Accepted: 28 October 2021; Published: 27 December 2021

Abstract

Mercury (Hg^{2+}) ion is considered as one of the most lethal heavy-metal contaminants accounting for its extreme persistence, bioaccumulation, and toxicity. The objective of this study is to synthesize hybrid carbon quantum dots (h-CQDs) for the detection of Hg^{2+} ion in purified water and simulated seawater using ratiometric fluorescence assay between blue carbon quantum dots(b-CQDs) produced from *Tamarindus indica* leaves and green carbon quantum dots(g-CQDs) produced from *Mangifera indica* leaves. The optical properties of the produced CQDs were determined using UV-Vis spectrophotometer which explained the quenching of g-CQDs' photoluminescence and stability of b-CQDs upon addition of Hg^{2+}. The research also includes the effect of volume ratio and time of microwave irradiation in the photoluminescence intensity ratio of h-CQDs and the influence of increasing Hg^{2+} concentration in both purified water and simulated seawater. The mathematical correlation between PL intensity ratio and concentration was found to be a rational equation for both purified and simulated seawater. Using simulated seawater, the result showed in the model has no significant difference with the detected concentrations using atomic absorption spectroscopy. Furthermore, the generated model exhibits dynamic range between 394 ppb and 23.85 ppm.

Keywords: quantum dots, g-CQDs, b-CQDS, mercury detection, carbon quantum dots

Abstrak

Ion merkuri (Hg^{2+}) dianggap sebagai satu pencemar logam berat maut berdasarkan sifatnya yang kekal, bioakumulasi, dan ketoksikan. Objektif kajian ini ialah menyediakan sintesis titik kuantum karbon hibrid (h-CQDs) bagi pengesanan ion Hg^{2+} dalam air tulen dan simulasi air laut mengunakan ujian pendaflour ratiometrik di antara titik kuantum karbon biru (b-CQDs) di hasil dari daun *Tamarindus indica* dan titik kuantum karbon hijau (h-CQDs) dari daun *Mangifera indica*. Sifat optikal yang terhasil bagi CQDs telah ditentukan melalui spektrofotometer UV-Vis menjelaskan pelindapan fotoluminesens g-CQDs dan

kestabilan b-CQDs dengan penambahan Hg^{2+}. Kajian juga termasuk melihat kesan nisbah isipadu dan masa bagi penyinaran gelombang mikro dalam nisbah keamatan fotoluminesens h-CQDs dan pengaruh peningkatan kepekatan Hg^{2+} bagi kedua-dua air tulen dan simulasi air laut. Korelasi matematik di antara nisbah keamatan PL dan kepekatan telah di ketahui menjadi persamaan sepadan bagi kedua-dua air tulen dan simulasi air laut. Mengunakan simulasi air laut, hasil menunjukkan model memberikan perbezaan tidak signifikan bagi kepekatan yang dikesan melalui analisis spektroskopi serapan atom. Selanjutnya, model yang dihasilkan memberi julat dinamik antara 394 ppb dan 23.85 ppm.

Kata kunci: titik kuantum, g-CQDs, b-CQDS, pengesanan merkuri, titik kuantum karbon

Introduction

Water is the link that binds all living organisms and the source of life on Earth. But nowadays, contamination of heavy metals is of increasing worldwide concern. Among the heavy metals, mercury (Hg^{2+}) ion is considered as one of the most lethal heavy-metal contaminants accounting for its extreme persistence, bioaccumulation, and toxicity. Bioaccumulation of this toxic heavy metal leads to liver, kidney, and lungs failure, central nervous system disorder, Minamata disease, brain damage, and even death. Recently, many residents of Palawan Province in the Philippines showed symptoms of the disease in the 2nd quarter of year 2017. Such phenomenon has been caused by small-scale gold mining operations undergoing on the place. Moreover, the burning of coal industry approximately releases approximately 475 tons of mercury [1].

Mining is not the only route where mercury can find its way to the environment. It also enters through industrial pathways including steel scrap processing facilities, coalfired plants, and the petroleum industry knowing to the fact that it is naturally produced due to its presence virtually all oil and gas. Mercury levels in crude oil and gas can vary widely, both between and within reservoirs and geographical areas. The rough introduction of mercury in the ecosystem alarms the public knowing that this hazard is not detectable by the human eye when dissolved in water and can cause serious environmental and health damage [1].

According to the US Environmental Protection Agency, the maximum allowable level of Hg^{2+} is 10 nm while the DENR AO 35 recommended amount of 5 ppb. Hence, it is a challenge to develop an accurate and sensitive analytical method in detecting trace amount of Hg^{2+} in water samples. Contemporarily, more than a few sophisticated analytical methods have been available for mercury monitoring including atomic absorption spectroscopy (AAS), electrochemical and optical sensing devices. Nonetheless, such a method requires sophisticated and expensive instrumentation, a long time of accomplishment, and complex sample pretreatment procedures. To combat the dilemma in producing results in a more portable, inexpensive, and time saving manner, many researchers used fluorescent nanoparticles specifically quantum dots [2].

Quantum dots were greatly utilized in recent years because of their attractive qualities and their versatile use in medicine, energy production, and heavy metal detection. Fluorescent metal quantum dots have been studied owing to their low toxicity and exceptional photostability. However, the production of these metal nanoparticles requires costly reagents, such as peptides, metal salts, proteins, polymers, thiol ligands and so on, which may limit their preparations and applications [3].

One of the techniques used in heavy metal detection using carbon quantum dots is ratiometric fluorescence assay because it is more reliable in the complex sample detection by determining the ratio of two signals where it can lessen the influence of instruments and environmental interference. In this study the researchers combined b-CQDs and g-CQDs to produce h-CQDs. In the addition of Hg^{2+}, the fluorescence of g-CQDs was quenched while the photoluminescence of the blue-emitting carbon remained the same [4].

To address the concerns for an inexpensive, nontoxic, reliable and rapid sensing system of mercury detection in purified water and simulated seawater, the

researchers used h-CQDs produced from *Tamarindus indica* leaves and *Mangifera indica* leaves. It is easy to fabricate, easy to operate, requires small sample volume, and has short response time. With the aid of h-CQDs, the ratiometric fluorescent sensor was able to display discernable color evolution from green to blue with increasing the concentration of Hg^{2+} [4].

Materials and Methods

Preparation of raw materials

Young *Mangifera indica* and *Tamarindus indica* leaves from the 3-5th internode of branches were collected at Panghayaan, Taysan, Batangas, Philippines. Initially, young plant leaves were taken and washed with water to remove dirt. Then, it was cut down into small pieces of size 1-2 cm. $HgCl_2$, the source of Hg^{2+}, was purchased in RTC Laboratory Services & Supply House Supplier while ethanol was procured in Belman Laboratories in Sheridan, Mandaluyong, Metro Manila. Lastly, chemicals for simulated seawater were bought in Lipa Quality Control Center in Lipa City, Batangas [5].

Preparation of green-emitting carbon quantum dots

An amount 70 grams of the *Mangifera indica* leaves have undergone leaching in 700 mL of absolute ethanol: water (1:1) by volume [5]. The mixture was stirred constantly for 4 hours and the resulting extract was transferred into a carbon steel reactor. The reactor was heated in the oven for 4 hours at 180°C and cooled down to room temperature for about 30 minutes. After cooling, the resulting solution undergone centrifugation at 4000 rpm for 30 minutes to obtain a clear supernatant [6]. The extract was further filtered to remove light particles with considerable volume [6]. Consequently, the purified solution was diluted to 400mL.

Preparation of blue-emitting carbon quantum dots

14 grams of the *Tamarindus indica* leaves was dissolved into 350 mL of distilled water. Accordingly, it was transferred into a carbon steel reactor and was kept for 5 hours at 210 ºC in the furnace. The obtained solution was cooled down to room temperature and centrifuged to 4,000 rpm for 30 minutes. To standardize the concentration, the resulting solution was diluted to the former volume of 350 mL [7].

Preparation of the simulated seawater

One liter (1L) of simulated seawater was prepared by emulating typical seawater with salinity of approximately 3%. Some of the components however was removed like most of the rare metals and heavy metals and the majority of the ionic compounds were only used. Because of solubility in water, the compounds were assumed to be completely dissociated into its ions to account for its elemental analysis. Table 1 below showed the formulation of simulated seawater [1].

Preparation of Hg^{2+} standard solution in purified water and seawater

Mercuric chloride ($HgCl_2$) was the source of Hg^{2+}. 1 gram of $HgCl_2$ was dissolved in 250 mL of purified water and seawater respectively to form 4,000 ppm standard solutions. 100 mL of the resulting solution was diluted to 250 mL of each to form 160 ppm standard solution. From the latter solution, the increasing concentration tabulated in Table 2 (447 ppb, 558 ppb, 1.397 ppm, 2.794 ppm, 4.191 ppm, 5.588 ppm, and 11.176 ppm) of $HgCl_2$ was prepared through the dilution method. The magnetic stirrer running at 3000 rpm facilitated the uniform concentration at 200 °C.

UV-Vis spectrophotometer calibration

The Shimadzu UV-1800 UV-Vis Spectrophotometer from Batangas State University, Philippines was switched on for 20 minutes for stabilization. Then, cuvettes were filled with purified water for the sample and kept sure that the outside was free from contamination. This has served as a blank and helped account for light losses due to scattering or absorption by the solvent. Afterwards, the cuvette was placed in the spectrometer. The cuvettes were aligned properly, as often the cuvette has two sides, which were meant for handling and were not meant to shine light through. The instrument stored the blank data and automatically performed the subtraction [8].

Absorbance spectrum collection and absorption peaks determination

The cuvettes were filled with the sample. It was rinsed twice with the sample for about ¾ full to make sure that the transfer is quantitative. Then it was placed in the spectrometer in the correct direction. The spectrum of absorbance was collected by scanning the instrument in wavelengths of 190 nm to 1100 nm. A diode-array instrument can collect the whole absorbance spectrum in one run. On the other hand, the absorption peaks were determined [9].

Functional group and conjugation determination using UV-Vis spectrophotometer

Determining functional groups and conjugation present in b-CQDs and g-CQDs helped researchers in explaining the color they emitted and their reactivity to Hg^{2+}. The presence of oxygen-rich group and electron withdrawing nitrogen atoms were responsible in the blue emission of b-QCDs in *Tamarindus indica* leaves whereas the presence of C=O and C-O-C groups in *Mangifera indica* leaves caused the green emission of g-QCDS including its the stability and reactivity to Hg^{2+}. Functional groups and conjugations were obtained from corresponding absorption peaks as shown in Table 3 [7].

Photoluminescence sensitivity enhancement of h-CQDs by microwave irradiation

80 mL of g-CQDs and b-CQDs, which were in a separate container, undergone microwave irradiation at a different time of exposure presented in Table 4. 800W microwave radiation at medium high power was used. After irradiating, the resulting solution was cooled and diluted with distilled water to restore its initial volume. For mass volume ratio, a specific volume of green and blue CQDs was mixed.

An additional setup with no exposure to microwave radiation was prepared to serve as the control [11].

Table 1. Seawater formulation for one liter of distilled water

Salt	Molecular Weight	Mass of Salt (g/kg solution)
Sodium chloride (NaCl)	58.44	23.926
Magnesium chloride ($MgCl_2.6H_2O$)	203.33	10.831
Sodium sulfate (Na_2SO_4)	142.04	4.008
Calcium chloride ($CaCl_2.H_2O$)	147.03	1.519
Potassium chloride (KCl)	74.56	0.677
Sodium bicarbonate ($NaHCO_3$)	84.00	0.196
Potassium bromide (KBr)	119.01	0.098
Boric acid (H_3BO_3)	61.83	0.026
Sodium fluoride (NaF)	41.99	0.003

Table 2. $HgCl_2$ concentration and corresponding Hg^{2+} ion concentration

$HgCl_2$ (ppm)	**Hg^{2+} (ppm)**
1.4	0.782
2.1	1.173
2.8	1.565
3.5	1.956
7.5	4.191
15	8.382
30	16.764

Table 3. Absorption peaks and corresponding chromophore, transition, and ε_{max}

Chromophore	**Transition**	**ε_{max}**	**λ_{max} (nm)**
σ – bonded electrons			
(C-C, C-H etc.)	σ-σ*		~ 150
Lone pair electrons			
-O-, -N-, -S-	n-σ*	100-1000	~ 190
C=O, C=N	n-π*	15	~300
	π-π*	500	~190
R-C=N	n-π*	5	~ 170
R-COOH, $RCONH_2$, RCOOR	n-π*	50	~ 210
π- bonded electrons			
C=C	π-π*	14000	~ 190
C=C	π-π*	2000	~ 195
C=O	π-π*	500	~ 180

Table 4. Variation of h-CQDs in purified water in terms of volume ratio of b-CQDs and g-CQDs and time of irradiation

Volume Ratio	**g-CQDs (mL)**	**b-CQDs (mL)**	**Time (minutes)**
1:2	40	80	
1:1	60	60	5, 10, 15
2:1	80	40	

Photoluminescence intensity ratio metering of 447 ppb Hg^{2+}

Hg^{2+} detection was performed at room temperature. In a typical detection experiment, 3 mL of varied h-CQDs dispersion and 3 mL of 447 ppb concentration of Hg^{2+} were mixed into 15 mL vials. After mixing thoroughly, the fluorescence spectra were recorded after 8 minutes of reaction at room temperature. The fluorescence

intensity ratio was measured at the excitation wavelength of 365 nm using UV light [10].

Luminous intensity metering setup

To capture light frequency, photos of the carbon quantum dots were taken using iPhone 8 Plus and images were converted to green and blue luminous intensity using Image J Batch Software [12]. For the smartphone fluorometer set-up, an enclosed chamber was equipped with 365 nm UV light which was showed in Figure 1. After putting the samples inside UV–chamber, a mobile phone camera was employed to capture images [13]. In order to block background light, a good image capturing angle was selected [13]. The captured images were then processed using RGB Measure plugin in ImageJ software wherein emission intensity from various samples was measured and compared adequately at the same time [13].

Figure 1. Luminous intensity metering set up

Photoluminescence intensity ratio metering in purified water and seawater

Set-up in metering photoluminescence of h-CQDs in 447 ppb was also used in metering purified water and seawater in increasing mercury concentration. In a typical detection experiment, 3 mL of defined amount of h-CQDs and 3 mL of known concentration of Hg^{2+} were added into 15-mL vials. After mixing thoroughly, the fluorescence spectra were recorded after reaction for 8 min at room temperature. The fluorescence intensity ratio was measured at the excitation wavelength of 365 nm UV light [10].

Statistical treatment

Empirical models and data curves relating the photoluminescence intensity ratio and the increasing concentration of Hg^{2+} heavy metal were constructed using MATLAB R2011-A which was a part of the last step in the schematic roadmap of the research methodology showed in Figure 2. Two paired t-test was performed to obtain the comparability degree between the photoluminescence ratios detected in purified water with that of seawater. On the other hand, analysis of variance was used to determine the effect of two variables namely mass ratio of h-CQDs and time of irradiation in the photoluminescence ratio change.

Validation of generated model using atomic absorption spectroscopy

To validate the degree of acceptability of the generated models low, medium and extreme concentrations for each type of heavy metal in simulated seawater were prepared prior to AAS testing. Tabulated in Table 5, Hg^{2+} (ppm) concentration variations were 0.335, 2.794, and 16.764.

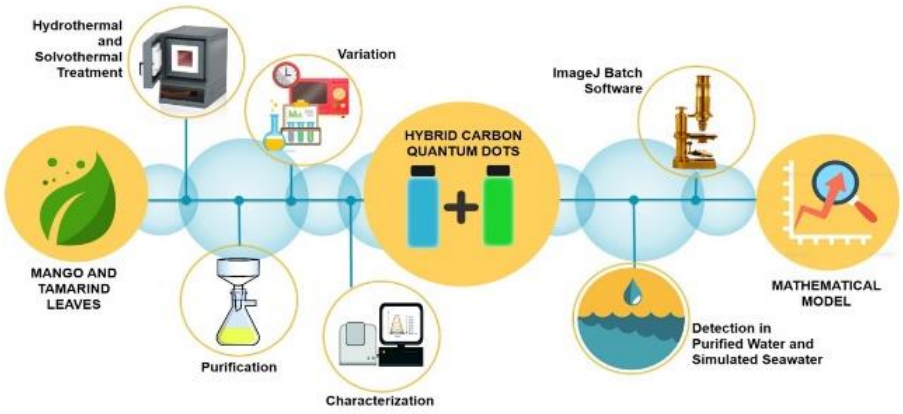

Figure 2. Schematic roadmap of the research methodology

Table 5. $HgCl_2$ low, medium, and extreme concentrations and corresponding Hg^{2+} concentration

$HgCl_2$ (ppm)	Hg^{2+} (ppm)
0.7	0.391
3.5	1.956
40	22.352

Results and Discussion

Determination of functional groups and conjugations present in g-CQDs and b-CQDs

In Figure 3, the absorption spectrum of g-CQDs showed distinct peaks at 191.5, 197.5, 208.5, 223.5, 235.5, 240.5, 253.0, 263.0 and 278.5 nm. The absorption peak of 208.5 nm corresponds to functional groups such R-COOH, $RCONH_2$, and RCOOR with the electronic transition of n - π*. The n electrons or the nonbonding electrons were the ones located on the oxygen of the carbonyl group. Thus, the n - π* transition corresponds to the excitation of an electron from one of the unshared pair to π* orbital. This requires the high energy of radiation among the detected functional groups due to the high energy requirement of the n and π* orbitals. However, the band energy gap between them was lower compared to the other detected functional groups.

Conversely, R-O-R, C=C, C=O were determined at 278.5 nm has energy transition from π to π* orbitals as shown in Table 6. These functional groups required more energy to excite electrons from π to π* orbitals. On the other hand, conjugate homoannular diene was defined at its peak of absorbance of 253 nm with an electronic transition from π_2 to π_3* orbital. In conjugated dienes the π–π* orbitals of the two alkene groups combine to form new orbitals – two bonding orbitals named as π_1 and π_2 and two anti-bonding orbitals named as π_3*and π_4*. It is apparent that a new π to π* transition of low energy is available as a result of conjugation. Conjugated dienes as a result absorb at relatively longer wavelength than do isolated alkenes. One component determined in the UV-Vis spectrum is gallic acid which was determined at its absorption peak at 263 nm. The oxygen containing functional groups such as C-O-C, and C=O groups, on the carbon backbone at the edge part were the typical source of the green luminescence in the CQDs [14].

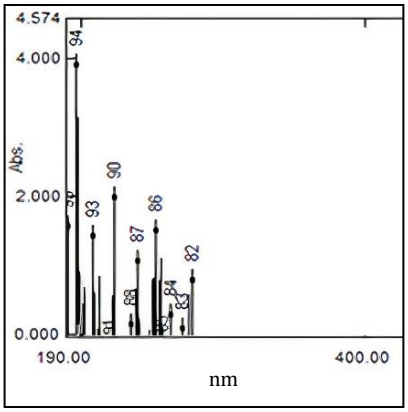

Figure 3. Wavelength and intensity of absorbance emission spectrum of g-CQDs

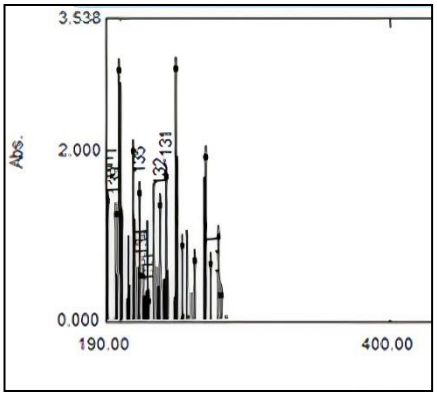

Figure 4. Wavelength and intensity of absorbance emission spectrum of b-CQDs

Figure 4 presents the optical properties of the synthesized b-CQDs which manifest a significant number of absorption peaks. At 209.5 nm, n - π* electronic transition is observed which is ascribed to several functional groups such as R-COOH, $RCONH_2$ and RCOOR. The lone electrons were located on the oxygen of the carbonyl group and responsible for the n orbital and excited to π* orbital. The high energy of radiation is required among the detected functional groups due to the high energy requirement of the n and π* orbitals. Though, the band energy gap between them is lower compared to the other detected functional groups. The absorption peak centered at 275 nm, the π-π* electronic transition of C=C is obtained. Blue emissive characteristics of b-CQDs were realized in the presence of oxygen-rich group and more electron withdrawing nitrogen atoms [7]. Table 7 tabulated the summary for functional groups and conjugation from optical properties of b-CQDs.

Comparison of photoluminescence intensity ratio of h-CQDs by the addition of Hg^{2+} upon varying volume ratio and time of irradiation

The PL intensity ratio of g-CQDs to b-CQDs was used to quantify the color change from blue to green upon addition of Hg^{2+}. A great increase in the PL Intensity Ratio corresponded to higher reactivity and detection capability to Hg^{2+}. The reaction between b-CQDs and g-CQDs was carried out using a 15 mL vial for 8 minutes. Prior to mixing, they have separately undergone microwave irradiation for 5, 10 and 15 minutes. An enclosed black chamber was used to ensure the absence of external lights while taking up pictures via a 12 MP smartphone. PL intensity ratio was measured using ImageJ Batch Software. In Table 8, PL intensity ratio of h-CQDs has increased upon addition of Hg^{2+} and produced different changes in varying volume ratio and time of irradiation. Meanwhile, Table 9 tabulated the difference in PL ratio listed in Table 8. In Figure 5 which was the illustration of Table 9, it was observed that the PL intensity ratio difference has increased when the volume ratio of b-CQDs to g-CQDs increased. Likewise, it has also increased when the time of irradiation was augmented. In addition, the highest PL intensity change of 0.0791 in Table 9 was obtained at 2:1 volume ratio and 15 minutes of irradiation. Therefore, h-CQD produced from these parameters was considered to be the best in detecting Hg^{2+}.

For the comparison of the PL ratio of h-CQDs in purified water with that of the contaminated water, the effect of varying volume ratio of b-CQDs and g-CQDS with a varying time of irradiation on the PL ratio was evaluated using analysis of variance. The confidence level was set to 0.05 wherein a p-value less than that depicts a significant change. Table 9 shows the statistical result.

It was shown in Table 10 that varying time of irradiation at fixed volume ratio produces p-value of 3.09×10^{-11} and F-stat value of 123.43. Conversely, varying volume ratios at the fixed time of irradiation yield p-value of 4.74×10^{-5} and f-stat value of 18.21. On the other hand, the varying time of irradiation and volume ratio at the same time, a p-value of 1.21×10^{-5} and f-stat of 15.44 were obtained. Since the p-value approaches 0 and f stat is larger than the F-critical value, this implies that varying the volume ratio and time of irradiation affects significantly the photoluminescence intensity ratio of h-CQDs.

Table 6. Functional groups and conjugations from optical properties of g-CQDs

Wavelength (nm)	**Intensity of Absorbance (abs)**	**Electronic Transition**	**Functional Group**	**Conjugation**	**Components Determined**
278.5	0.671	π–π*	C=O, C=C, R-O-R		
263.0	0.183				Gallic Acid
253.0	1.395	π_2 - π_3*		Homoannular Diene	
240.5	0.958				
235.5	0.045				
223.5	1.869				
208.5	1.313	n - π*	R-COOH, $RCONH_2$, RCOOR		
197.5	3.794				
191.5	1.456				

Table 7. Functional groups and conjugations from optical properties of b-CQDs

Wavelength (nm)	Intensity of Absorbance (abs)	Electronic Transition	Functional Group	Conjugation
275.0	0.201	π-π*		C=C
263.0	1.823			
241.5	2.853			
234.5	1.583			
229.5	1.261			
214.0	1.394			
209.5	1.882	n - π*	R-COOH, $RCONH_2$, RCOOR	
199.5	2.836			
197.0	1.151			
191.5	1.311			

Table 8. Photoluminescence ratio of h-CQDs with and without Hg^{2+} upon varying volume ratio and time of irradiation

Vol. Ratio	Time					
	5		10		15	
	Without Hg^{2+}	With Hg^{2+}	Without Hg^{2+}	With Hg^{2+}	Without Hg^{2+}	With Hg^{2+}
2:1	0.512	0.533	0.504	0.558	0.507	0.589
1:1	0.591	0.593	0.596	0.603	0.594	0.560
1:2	0.663	0.670	0.674	0.678	0.675	0.682

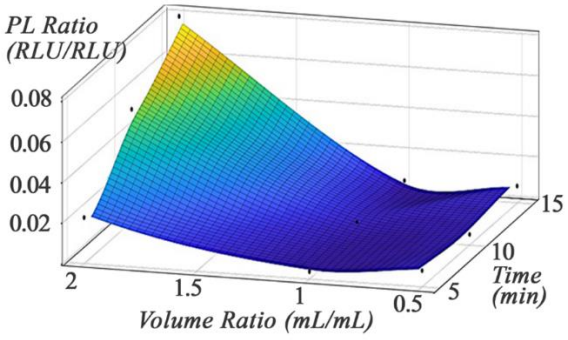

Figure 5. Illustration of photoluminescence ratio difference of h-CQDs by the addition of Hg^{2+} upon varying volume ratio and time of irradiation

Table 9. Photoluminescence ratio difference of h-CQDs upon varying volume ratio and time of irradiation

Ratio	Time		
	5	10	15
2:1	0.0215	0.0541	0.0791
1:1	0.0027	0.0062	0.0060
1:2	0.0070	0.0041	0.0072

Table 10. Statistical result for the effect of varying volume ratio and time of irradiation of b-CQDs and g-CQDs

Set-up	Mean Square	Sum of Squares	F-stat	p-value	F-critical
Time of Irradiation	6.363×10^{-3}	1.27×10^{-2}	123.43	3.09×10^{-11}	3.55
Volume Ratio	9.39×10^{-4}	1.88×10^{-3}	18.21	4.74×10^{-5}	3.55
Time of Irradiation and Volume Ratio	7.96×10^{-4}	3.19×10^{-3}	15.44	1.21×10^{-5}	2.93

Note: p-value depicts a value greater than a = 0.05 has no significant effect

Determination of PL intensity ratio of h-CQDs upon increasing Hg^{2+} concentration in purified water and simulated seawater

It was observed in the Table 11 that as concentration of mercury ion was increased from 0.782 ppm to 16.764 ppm, the PL intensity ratio of b-CQDs to g-CQDs for purified water increased from 0.5867 to 1.1052. On the other hand, in the same range of concentration, the PL intensity ratio for simulated seawater increased from 0.5590 to 0.9217. In purified water, there was a 79.31% increase in the PL intensity ratio and using simulated seawater as the medium, 64.88% increase in PL intensity ratio was realized. PL intensity ratios of h-CQDs with the increasing Hg^{2+} concentration in purified and simulated seawater were illustrated in Figure 7 and Figure 8 respectively.

Since the PL ratio pertains to the ratio of photoluminescence of b-CQDs to g-CQDs, an increase in this value means a decrease in the sole photoluminescence of g-CQDs because it has the ability to quench with mercury [14] who synthesized bluish green emitting carbon quantum dots and has proven its mercury ion sensing application. The color transition upon quenching mercury was illustrated in Figure 6. It was proven that blue-emissive carbon quantum dots derived from tamarind leaves exhibit sensitivity only to glutathione [7], thus, unreactive to Hg^{2+}. So, the increase in PL Ratio was associated with the increase in mercury concentration creating a higher degree of quenching of the g-CQDs.

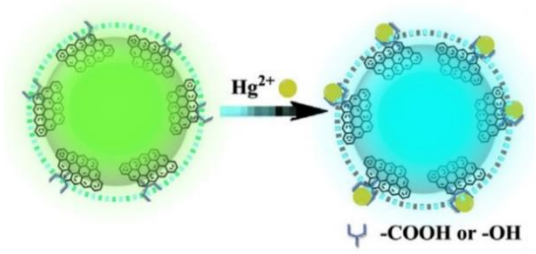

Figure 6. Quenching mechanism

Using purified water as the medium, a p-value of 1.65×10^{-10} and F-stat of 1491.58 were obtained as seen in Table 12. On the other hand, using simulated seawater, a p-value of 7.47×10^{-11} and F-stat value of 1871.03 were obtained. Since p ~ 0 and F-stat possessed a value higher than F-critical, this implies that an increase in

Hg^{2+} concentration in both medium affects significantly the photoluminescence intensity ratio of the h-CQDs.

Table 13 tabulated the statistical comparison of the photoluminescence intensity ratio of h-CQDs in purified water and simulated seawater. The analysis resulted to a p-value of 2.36×10^{-6} and a t -value of 6.519. Since the p-value is lower than the set confidence of 0.05, the difference between the experimental PL ratios of the two media upon increasing Hg^{2+} concentrations is significant.

Table 11. PL intensity ratio of h-CQDs with the increasing Hg^{2+} concentration in purified water and simulated seawater

$HgCl_2$ Concentration (ppm)	**Hg^{2+} Concentration (ppm)**	**Photoluminescence Intensity Ratio**	
		Purified Water	**Simulated Seawater**
1.4	0.782	0.5867	0.5590
2.1	1.173	0.6531	0.6101
2.8	1.565	0.7164	0.6655
3.5	1.956	0.7849	0.7221
7.5	4.191	0.8583	0.8151
15	8.382	0.9541	0.8661
30	16.764	1.1052	0.9217

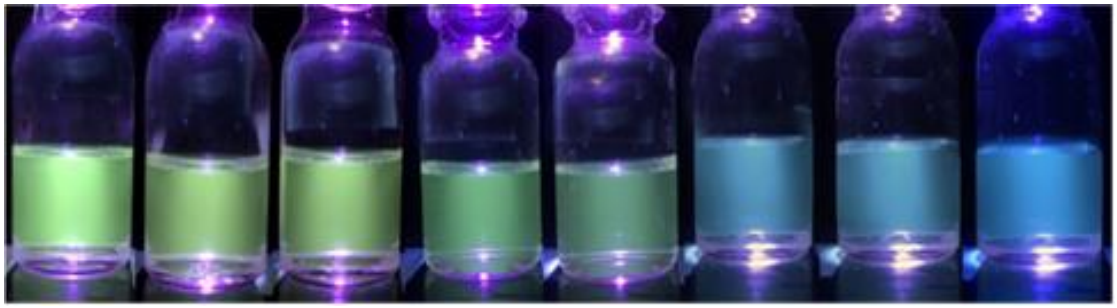

Figure 7. Color progression of h-CQDs with the increasing Hg^{2+} concentration in purified water

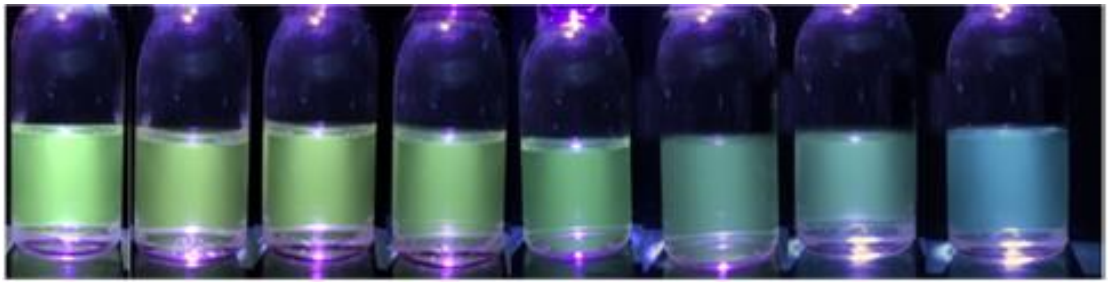

Figure 8. Color progression of h-CQDs with the increasing Hg^{2+} concentration in simulated seawater

Table 12. Statistical result for the effect in PL intensity ratio of h-CQDs upon increasing Hg^{2+} concentration in purified water and simulated seawater

Medium	Mean Square	Sum of Squares	F-stat	p-value	F-critical
Purified Water	6.43×10^{-2}	0.3856	$1.492 \times 10^{+3}$	1.65×10^{-10}	3.87
Simulated Seawater	3.67×10^{-2}	0.2202	$1.871 \times 10^{+3}$	7.47×10^{-11}	3.87

Note: p-value depicts a value greater than a = 0.05 has no significant effect.

Table 13. Statistical result for the comparison of PL intensity ratio of h-CQDs in purified water and simulated seawater

Standard Deviation	Mean Difference	t-value Mean	t-Critical value	p-value	Standard Error
-	7.171×10^{-2}	6.519	2.086	2.36×10^{-6}	-

Note: p-value depicts a value greater than a = 0.05 has no significant effect

Correlation model on the effect of Hg^{2+} concentrations to photoluminescence ratio of h-CQDs in purified water and simulated seawater

In choosing the best mathematical model from the generated equation presented in Tables 14 and 15, the fitness of equation must be met in terms of the sum of squared error (SSE), the adjusted, and root mean squared error. Likewise, the best fit was the model with the lowest SSE and RMSE because this measures the errors from the data points. With respect to R^2, the model closest to one is the fittest. From the generated equation, the equation with the lowest SSE and RMSE for the purified water are Fourier and Rational equations. In consideration of the R^2 and adjusted R^2 values, it also has the closest value to 1.

However, another factor to consider in the selection of the best fit was the asymptote or minimum value of photoluminescence ratio as the heavy increases and approaches infinity and the maximum value as heavy metal concentration approaches 0. By the evaluation of the above equations, Fourier, Gauss, and 3rd degree polynomial exhibit fluctuating trends. Thus, in 2 different x values, there is one y value. This tells that the model greatly deviates the ideal model. With respect to 2nd power exponential, higher value of concentration corresponds to photoluminescence intensity ratio of 10 which is far from the typical range of PL Ratio. This concludes that the rational equation was the best fit because it has the least negative value as concentration approaches infinity aside from exhibiting the highest R^2 and least value of SSE and RMSE.

Comparison of the Hg^{2+} concentration calculated from the generated model with the detected concentrations using AAS

In Table 16, the amount of concentration calculated from the selected model was summarized. With the increase in formulated concentration, the photoluminescence intensity ratio was also increased. Relative to the detected concentration from AAS, the calculated concentration using the model provided values that are nearly the same with maximum deviation (by difference) of 1.4010 and minimum deviation of 0.0255. Also, the model fits more effectively at low to moderate concentrations.

In Table 17, the p-value calculated was greater than 0.05 which denotes the acceptance of the null hypothesis. Thus, there was no significant difference between Hg^{2+} concentrations calculated from the generated mathematical model with that detected of the AAS.

Table 14. Generated model curves describing the effect of Hg^{2+} concentrations to PL intensity ratio of h-CQDs in purified seawater

Types of Model Fit	Method	Equations Generated	SSE	R^2	Adjusted R^2	RMSE
Exponential (2nd Power)	Non-linear Squares	$P(C)= 0.8896e^{0.1094C} - 0.003685e^{-5.82C}$	7.40 x 10^{-4}	0.9962	0.9925	1.57 x 10^{-2}
Fourier (2nd Power)	Non-linear Squares	$P(C)=$ 0.8512 - 0.1936cos(0.6066*C) - 0.1212sin(0.6066*C) - 0.1217cos(1.2132*C) + 0.04304sin(1.2132*C)	2.309 x 10^{-5}	0.9999	0.9993	4.81 x 10^{-3}
Gauss (2 terms)	Non-linear Squares	$P(C)= 4.281e^{(\frac{12.83-C}{3.382})^2} + 0.8857e^{(\frac{3.401-C}{4.055})^2}$	6.226 x 10^{-5}	0.9997	0.9981	7.89 x 10^{-3}
Linear Model	Linear Squares	$P(C)= 0.0005877C^3 - 0.01678C^2 + 0.1522C + 0.5034$	3.86 x 10^{-3}	0.9803	0.9607	3.59 x 10^{-2}
Power	Non-linear Squares	$P(C)= -13.05C^{-0.01258} + 13.69$	2.87 x 10^{-3}	0.9853	0.978	2.68 x 10^{-2}
Rational	Linear Squares	$P(C)= \frac{1.472C^3 - 1.594C^2 - 9.234C + 32.33}{5.6C^2 - 36.38C + 66.7}$	1.855 x 10^{-5}	0.9999	0.9995	4.31 x 10^{-3}

Table 15. Generated model curves describing the effect of Hg^{2+} concentrations to PL intensity ratio of h-CQDs in simulated seawater

Types of Model Fit	Method	Equations Generated	SSE	R^2	Adjusted R^2	RMSE
Exponential (2nd Power)	Non-linear Squares	$P(C)= 0.8168e^{0.007198C} - 0.007198e^{-5.82C}$	2.99 x 10^{-4}	0.9973	0.9946	9.98 x 10^{-3}
Fourier (2nd Power)	Non-linear Squares	$P(C)=$ 1.163 - 0.4006cos(0.331*C) - 0.6585sin(0.331*C) - 0.2602cos(0.662*C) + 0.3601sin(0.662*C)	5.70 x 10^{-7}	1	1	7.55 x 10^{-4}
Gauss (2 terms)	Non-linear Squares	$P(C)= 1.864e^{(\frac{13-C}{4.485})^2} + 0.8e^{(\frac{3.43-C}{4.363})^2}$	6.478 x 10^{-7}	0.9994	0.9965	8.05 x 10^{-3}
Linear Model	Linear Squares	$P(C)= 0.0005711C^3 - 0.0169C^2 + 0.1485C + 0.4654$	1.32 x 10^{-3}	0.988	0.9761	2.09 x 10^{-2}
Power	Non-linear Squares	$P(C)= -0.4904C^{-0.385} + 1.088$	7.68 x 10^{-4}	0.993	0.9895	1.39 x 10^{-2}
Rational	Linear Squares	$P(C)= \frac{1.01C^3 - 2.377C^2 - 0.8211C + 9.568}{-0.4871C^2 - 9.038C + 21.16}$	4.286 x 10^{-5}	1	1	0

Table 16. Concentration of Hg^{2+} based on calculated and detected values

Formulated Hg^{2+} concentration (ppm)	Photoluminescence Intensity Ratio	Calculated Concentration using the Model (ppm)	Detected Concentration
0.3912	0.5140	0.4347	0.3940
1.9558	0.7214	1.9455	1.92
22.3517	0.9415	22.4490	23.85

Table 17. Statistical result for the comparison of calculated and detected concentration of Hg^{2+} in simulated seawater

Standard Deviation	Mean Difference	t-Value	t-Critical Value	p-Value	Standard Error Mean
-	0.45821	1.574	2.306	1.54×10^{-1}	-

Note: p-value depicts a value greater than a = 0.05 has no significant effect

.

Conclusion

The following conclusions were based on the mathematical analysis of the data using the appropriate computer software and the in-depth interpretation of the results and findings. Oxygen-rich group and electron withdrawing nitrogen atoms in *Tamarindus indica* leaves were responsible for the blue-emission of b-QCDs whereas the presence of C=O and C-O-C groups in *Mangifera indica* leaves contributed in the green color emission of b-CQDs, its stability to simulated seawater electrolytes and selective reactivity to Hg^{2+}. Varying the volume ratio of blue to green carbon quantum dots and the time of irradiation played a significant role in mercury detection. Simulated seawater salts inhibited the quenching of green carbon quantum dots with mercury affecting its photoluminescence intensity. The generated mathematical models have been tested to be a reliable tool in determining Hg^{2+} concentrations at a specific range with no significant difference with the AAS detected concentrations.

Acknowledgement

The researchers would like to express their gratitude and appreciation to Batangas State University Alangilan for allowing them to maximize its full potential as an experimental laboratory workplace; To PIChE National for giving this research a breakthrough last February 2019 and to all the people who interceded for the success of this research

References

1. Guo, Y., Wang, Z., Shao, H. and Jiang, X. (2013). Hydrothermal synthesis of highly fluorescent carbon nanoparticles from sodium citrate and their use for the detection of mercury ions. *Carbon,* 52: 583-589.
2. World Health Organization (2017). Mercury and health. Retrieved from https://www.who.int/news-room/fact-sheets/detail/mercury-and-health.
3. Guo, X., Liu, C., Li, N., Zhang, S. and Wang, Z. (2018). Ratiometric fluorescent test paper based on silicon nanocrystals and carbon dots for sensitive determination of mercuric ions. *Royal Society Open Science,* 5(6): 171922.
4. Rajendran, K. and Rajendiran, N. (2018). Bluish green emitting carbon quantum dots synthesized from jackfruit (*Artocarpus heterophyllus*) and its sensing applications of Hg(II) and Cr(VI) ions. *Materials Research Express,* 5(2): 024008.

5. Lu, W., Qin, X., Liu, S., Chang, G., Zhang, Y., Luo, Y., Asiri A., Al-Youbi A. and Sun X. (2012). Economical, green synthesis of fluorescent carbon nanoparticles and their use as probes for sensitive and selective detection of mercury(II) ions. *Analytical Chemistry,* 84(12): 5351-5357.
6. Canson, M., Cantos, J. and de Guzman, M. (2016). Modelling the effect of varying Cr^{6+} And Cu^{2+} concentration on the luminous intensity of photobacterium phosphoreum in simulated seawater. Alangilan, Batangas City: Batangas State University.
7. Bano, D., Kumar, V., Singh, V. and Hasan, S. (2018). Green synthesis of fluorescent carbon quantum dots for the detection of mercury(II) and glutathione. *New Journal of Chemistry,* 42(8): 5814-5821.
8. Ma, Y., Zhang, Z., Xu, Y., Ma, M., Chen, B., Wei, L. and Xiao, L. (2016). A bright carbon-dot-based fluorescent probe for selective and sensitive detection of mercury ions. *Talanta,* 161, 476-481.
9. Bhati, A., Anand, S. R., Gunture, Garg, A. K., Khare, P. and Sonkar, S. K. (2018). Sunlight-induced photocatalytic degradation of pollutant dye by highly fluorescent red-emitting Mg-N-embedded carbon dots. *ACS Sustainable Chemistry & Engineering,* 6(7): 9246-9256.
10. Mu, Q., Li, Y., Xu, H., Ma, Y., Zhu, W. and Zhong, X. (2014). Quantum dots-based ratiometric fluorescence probe for mercuric ions in biological fluids. *Talanta,* 119: 564-571.
11. JoVE Science Education Database (2021). Ultraviolet-visible (UV-Vis) spectroscopy. JoVE, Cambridge, MA. Retrieved from https://www.jove.com/v/10204/ultraviolet-visible-uv-vis-spectroscopy.
12. Kumawat, M., Thakur, M., Gurung, R. and Srivastava, R. (2017). Graphene quantum dots from *Mangifera indica*: Application in near-infrared bioimaging and intracellular nanothermometry. *ACS Sustainable Chemistry & Engineering,* 5(2), 1382-1391.
13. Bagheri, Z., Ehtesabi, H., Rahmandoust, M., Ahadian M. M., Hallaji Z., Eskandari F. and Jokar E. (2017). New insight into the concept of carbonization degree in synthesis of carbon dots to achieve facile smartphone based sensing platform. *Scientific Report,* 7: 11013.
14. Tchounwou, P. B., Yedjou, C. G., Patlolla, A. K. and Sutton, D. J. (2012) Heavy Metal Toxicity and the Environment. In: Luch A. (Ed.) Molecular, Clinical and Environmental Toxicology. Experientia Supplementum, Springer, Basel: pp. 133-164.